Cell-based screen for altered nuclear phenotypes reveals senescence progression in polyploid cells after Aurora kinase B inhibition

Mahito Sadaie[a,*], Christian Dillon[b,†], Masako Narita[a], Andrew R. J. Young[a], Claire J. Cairney[c], Lauren S. Godwin[d], Christopher J. Torrance[e], Dorothy C. Bennett[d], W. Nicol Keith[c], and Masashi Narita[a]

[a]Cancer Research UK Cambridge Institute, University of Cambridge, Cambridge CB2 0RE, United Kingdom; [b]Cancer Research Technology Discovery Laboratories, Wolfson Institute for Biomedical Research, London WC1E 6BT, United Kingdom; [c]Institute of Cancer Sciences, Wolfson Wohl Cancer Research Centre, University of Glasgow, Glasgow G61 1QH, United Kingdom; [d]St. George's, University of London, London SW17 0RE, United Kingdom; [e]Horizon Discovery Ltd, IQ Cambridge, Waterbeach, Cambridge CB25 9TL, United Kingdom

ABSTRACT **Cellular senescence is a widespread stress response and is widely considered to be an alternative cancer therapeutic goal. Unlike apoptosis, senescence is composed of a diverse set of subphenotypes, depending on which of its associated effector programs are engaged. Here we establish a simple and sensitive cell-based prosenescence screen with detailed validation assays. We characterize the screen using a focused tool compound kinase inhibitor library. We identify a series of compounds that induce different types of senescence, including a unique phenotype associated with irregularly shaped nuclei and the progressive accumulation of G1 tetraploidy in human diploid fibroblasts. Downstream analyses show that all of the compounds that induce tetraploid senescence inhibit Aurora kinase B (AURKB). AURKB is the catalytic component of the chromosome passenger complex, which is involved in correct chromosome alignment and segregation, the spindle assembly checkpoint, and cytokinesis. Although aberrant mitosis and senescence have been linked, a specific characterization of AURKB in the context of senescence is still required. This proof-of-principle study suggests that our protocol is capable of amplifying tetraploid senescence, which can be observed in only a small population of oncogenic RAS-induced senescence, and provides additional justification for AURKB as a cancer therapeutic target.**

Monitoring Editor
Robert D. Goldman
Northwestern University

Received: Jan 5, 2015
Revised: May 22, 2015
Accepted: Jun 23, 2015

This article was published online ahead of print in MBoC in Press (http://www.molbiolcell.org/cgi/doi/10.1091/mbc.E15-01-0003) on July 1, 2015.

Present addresses: *Graduate School of Biostudies, Kyoto University, Kyoto 606-8501, Japan; †London Bioscience Innovation Centre, London NW1 0NH, United Kingdom.

Address correspondence to: Masashi Narita (Masashi.Narita@cruk.cam.ac.uk).

Abbreviations used: AURK, aurora kinase; BrdU, 5-bromo-2′-deoxyuridine; DAPI, 4′,6-diamidino-2-phenylindole; DMSO, dimethyl sulfoxide; H3S10ph, histone H3 phosphorylated at serine 10; HDF, human diploid fibroblast; IRG, hit compound that induces an irregular nuclear shape; SA-β-gal, senescence-associated β-galactosidase; SAC, spindle assembly checkpoint; SAHF, senescence-associated heterochromatic foci; SASP, senescence-associated secretory phenotype; SPT, hit compound that induces spotty morphologies; TIS, therapy-induced senescence.

INTRODUCTION

Cellular senescence is a state of stable or "irreversible" cell cycle arrest induced by various cytotoxic factors, including telomere dysfunction, DNA damage, oxidative stress, oncogenic stress, and some types of cytokines (Correia-Melo *et al*., 2014; Salama *et al*., 2014) Although senescence was originally defined in normal human diploid fibroblasts (HDFs)—the best-characterized culture model of senescence—a similar phenotype can be induced in a wide range of cell types, as well as in in vivo contexts that are associated with various pathophysiological conditions, such as tumorigenesis (Pérez-Mancera *et al*., 2014), tissue repair (Krizhanovsky *et al*., 2008; Jun and Lau, 2010), aging (López-Otín *et al*., 2013), and, more recently, embryogenesis (Chuprin *et al*., 2013; Muñoz-Espín *et al*., 2013; Storer *et al*., 2013). Of these, oncogene-induced senescence, in which excessive mitogenic stress provokes senescence effectors leading to progressive development of senescence phenotypes in

culture and animal models, underscores the tumor suppressor role of senescence. In addition, it has been shown that senescence can also be induced by chemotherapeutic reagents in tumors (therapy-induced senescence [TIS]), particularly in apoptosis-defective contexts (Poele *et al.*, 2002; Schmitt *et al.*, 2002; Xue *et al.*, 2007; Gewirtz *et al.*, 2008; Ewald *et al.*, 2010; Dörr *et al.*, 2013). Therefore senescence has been considered as not only an intrinsic tumor suppressor, but also an alternative therapeutic goal in cancer (Acosta and Gil, 2012; Cairney *et al.*, 2012). However, it has been shown that senescence may also facilitate tumorigenesis: senescent cells often secrete a wide range of soluble factors, which have a considerable effect on the tumor microenvironment and local immune response, providing antitumorigenic and/or protumorigenic effects, depending on the context (Coppé *et al.*, 2010; Pérez-Mancera *et al.*, 2014).

Senescence is typically a dynamic and long-term process, which can involve many regulatory effector mechanisms, conferring a diverse and heterogeneous nature on the phenotype (Salama *et al.*, 2014). Thus, to evaluate qualitatively the senescence phenotype, various cellular and biochemical markers have been identified. Senescence markers include accumulation of senescence-associated β-galactosidase (SA-β-gal) activity, a persistent DNA-damage response, the senescence-associated secretory phenotype (SASP; Kuilman and Peeper, 2009; Coppé *et al.*, 2010), and autophagy (Salama *et al.*, 2014). In addition, senescence is typically accompanied by an enlarged cellular morphology with increased vesicle formation. Senescent nuclei can also display distinct morphological changes, including an enlargement of the nuclei and the nucleoli (Mitsui and Schneider, 1976; Bemiller and Lee, 1978), formation of senescence-associated heterochromatic foci (SAHF; Narita *et al.*, 2003; Zhang *et al.*, 2005), up-regulation of promyelocytic leukemia nuclear bodies both in size and number (Ferbeyre *et al.*, 2000; Pearson *et al.*, 2000; Bischof *et al.*, 2002, 2005), alterations of lamin B1 and other components of the nuclear envelope (Maeshima *et al.*, 2006; Barascu *et al.*, 2012; Freund *et al.*, 2012; Dreesen *et al.*, 2013; Sadaie *et al.*, 2013; Shah *et al.*, 2013), and alterations of nuclear shape (Matsumura *et al.*, 1979; reviewed in Goldstein, 1990; Cristofalo and Pignolo, 1993). Hence it has been proposed that it is necessary to combine multiple markers, which can be either common or unique to different contexts. Validation of stable exit from the cell cycle is required for the phenotype to qualify as senescence (Campisi, 2013; Salama *et al.*, 2014).

Aurora kinase B (AURKB) is a member of the Aurora family, which also includes the related kinases AURKA and AURKC. Both AURKA and AURKB are ubiquitously expressed, but their subcellular localization, binding partners, and substrates are highly distinctive. The different isoforms are thus involved in different aspects of cell cycle regulation, whereas AURKC is mainly expressed in testis, and its function is not well characterized (Gautschi *et al.*, 2008). Whereas AURKA is a centrosomal protein, mainly related to centrosome function and bipolar spindle assembly, AURKB, the catalytic component of the chromosome passenger complex, plays a key role in correct chromosomal alignment and segregation by destabilizing erroneous kinetochore–microtubule attachments and is believed to be involved in the spindle assembly checkpoint (SAC). It also has a critical role in cytokinesis (Kelly and Funabiki, 2009; Lens *et al.*, 2010; Carmena *et al.*, 2012). Inhibition of AURKB in cell culture leads to a failure to biorient chromosomes and perturbed cytokinesis and, as a consequence, causes polyploidization and an eventual loss of viability (Ditchfield *et al.*, 2003; Kaestner *et al.*, 2009; Lens *et al.*, 2010). It was shown that AURKs inhibitors that are more selective for AURKA induce senescence in tumor cells (Huck *et al.*, 2010; Liu *et al.*, 2013). On the other hand, it was also shown that the ectopic expression of AURKB in normal HDFs induces senescence (Jung *et al.*, 2005). A more recent study, however, reported that AURKB overexpression delays senescence, and small interfering RNA–mediated AURKB knockdown induces senescence in HDFs (Kim *et al.*, 2011). Thus there is room for a more detailed characterization of the senescence phenotype caused by the modulation of AURKB expression and, more specifically, its enzymatic activity.

Owing to the diverse nature of senescence, identifying or developing senescence-inducing factors not only would extend our cancer therapeutic modalities, it would also help in elucidating the effector mechanisms of senescence. Although numerous genetic "senescence bypass" screens have been successfully conducted (Jacobs *et al.*, 2000; Shvarts *et al.*, 2002; Gil *et al.*, 2004; Acosta *et al.*, 2008; Kortlever *et al.*, 2008; Leal *et al.*, 2008; Rovillain *et al.*, 2011), attempts at "senescence-inducing" screens are limited (Ewald *et al.*, 2009; Lahtela *et al.*, 2013). Here, taking advantage of a high-content fluorescence image analyzing system, we set out simple primary screens for small molecules that can induce senescence-related nuclear phenotypes, namely an enlargement in nuclear size and SAHF-like chromatin spottiness, in HDFs, followed by secondary analyses for detailed senescence validation in both HDFs and tumor cell lines. Using a kinase inhibitor library, we identify compounds that induce senescence with different nuclear morphologies. Of interest, although the substrate specificities of the kinase inhibitors used were rather limited, a subset of the hit compounds converged on AURKB to induce a unique senescence phenotype, in which G1 tetraploidy or polyploidy progressively accumulated. Our study provides a simple and sensitive prosenescence screen, and the data reinforce the relevance of AURKB as a cancer therapeutic target.

RESULTS

Identification of small-molecule compounds that induce senescence-associated morphological changes in nuclei

To establish an image-based screen for senescence inducers, we focused on senescence-associated nuclear morphological changes as our readout, using high-throughput fluorescent microscopy (Figure 1A). We chose IMR90 HDFs, which are generally more sensitive to senescence than apoptosis in response to cellular stress and have thus been well characterized in terms of senescence (Serrano *et al.*, 1997; Narita *et al.*, 2003). To optimize the protocol for image acquisition and the analyses of nuclear size and nuclear foci (spots), we used normal and $HRAS^{G12V}$-induced senescent cells, which exhibit prominent SAHFs (Figure 1B; Narita *et al.*, 2003). Cells were plated on 96-well plates, fixed, and stained with 4′,6-diamidino-2-phenylindole (DAPI) for the automated imaging of nuclei (Supplemental Figure S1 and Supplemental Table S1).

Using this system, we treated normal proliferating IMR90 cells with 160 kinase inhibitors (InhibitorSelect; Calbiochem/Merck) and quantified both the nuclear size and the area of any subnuclear foci per nucleus (Figure 1C). The scores from each well were normalized to those from the dimethyl sulfoxide (DMSO) controls, and the hits were determined by setting a threshold of either 1.2-fold ("relative nuclear average area") or threefold ("relative spot total area per nucleus") above the control. Of 160 compounds (tested at a standardized 5 μM), 11 and 17, scored positive for nuclear size (large) and spottiness (spotty), respectively, with substantial overlap (Figure 1D and Supplemental Tables S2 and S3). Cells with an enlarged or spotty nucleus tended to show a low relative object count per field, which reflected the averaged cell density in the area scanned (Supplemental Figure S1C), suggesting that those hit compounds have antiproliferative and/or procell death activity. Similar results were

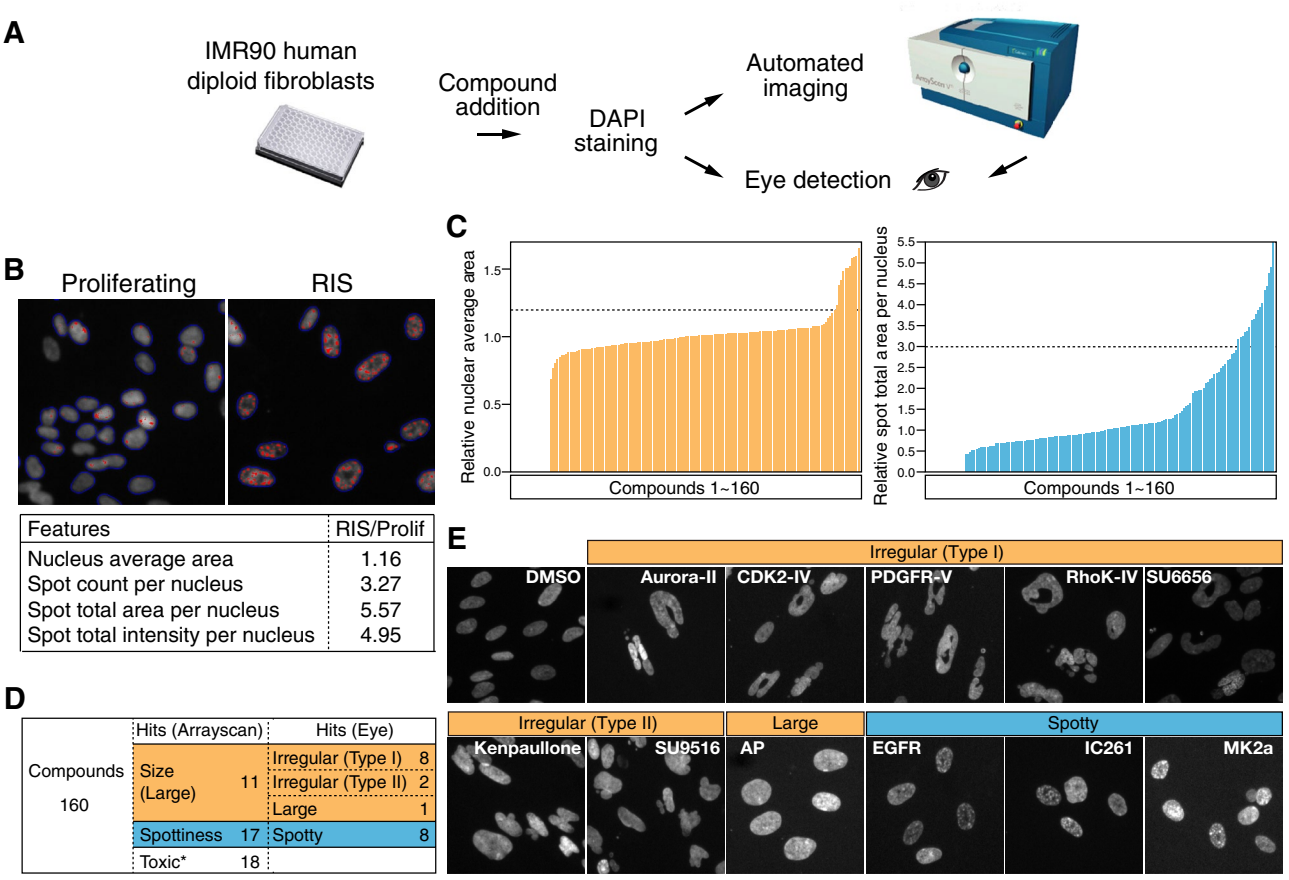

FIGURE 1: Automated image-based screening for compounds that induce morphological changes in nuclei. (A) Flow of the screen. Cells were treated with small-molecule kinase inhibitors for 4 d in 96-well plates, followed by fixation and staining with DAPI, and analyzed using an automated image analyzer (ArrayScan), along with a visual inspection by fluorescence microscopy. (B) The protocol for automated nuclear image acquisition and analyses was set up using normally proliferating and H-RAS^{G12V}–induced senescent (RIS) IMR90 cells. Nuclei (DAPI signals) were recognized in the first channel (marked with blue contours), and then any spotty pattern was detected in the second channel (marked in red). Numbers represent the ratios between RIS and proliferating (Prolif) cells for the indicated features. (C) Score distributions of the nuclear average area (left) or the spot total area per nucleus (right) of the cells after 4-d exposure to 5 μM compounds. Threshold was set at 1.2-fold (relative nuclear average area) or 3-fold (relative spot total area per nucleus) of a DMSO control. (D) Number of the hits identified by the automated detection and subsequent eye detection. Cells were treated as in C. Asterisks, toxic compounds that failed to give >100 nuclei count. (E) Representative fluorescence images of nuclei of the cells treated with hit compounds by ArrayScan. Enlarged nuclei are categorized into three types according to their shape: irregular type I, irregular type II, and large. AP, aminopurvalanol A; Aurora-II, Aurora kinase inhibitor II; CDK2-IV, CDK2 inhibitor IV; EGFR, EGFR inhibitor; MK2a, MK2a inhibitor; PDGFR-V, PDGF RTK inhibitor V; RhoK-IV, Rho kinase inhibitor IV.

obtained when we treated cells with the compounds at 3 μM (Supplemental Figure S1D).

We also manually scored all the compounds by visually inspecting the scanned images. The nuclei from the cells treated with the 11 size hits were all recognized as substantially enlarged, and the spotty nuclei in at least eight of 17 hits-treated cells were confirmed by eye. Of interest, in most of the size hits, the nuclei exhibited a severe malformation, with a fragmented, cashew nut–like, or doughnut-like morphology, often accompanied by multiple micronuclei (type I), whereas some showed milder changes and were without fragmentation or holes (type II; Figure 1E and Supplemental Figure S1E). The size hits also included nuclei without any apparent irregularity ("large"). We termed the hit compounds that induced an irregular nuclear shape and spotty morphologies IRGs and SPTs, respectively, and examined whether these phenotypes are associated with cellular senescence.

Hit compounds identified by the screen are capable of inducing cellular senescence

To determine whether the hit compounds induce senescence in IMR90 cells, secondary assays were performed for a subset of compounds: those that scored positive, as well as those that showed a stronger irregular phenotype (type I) in the screen (Figure 2). To optimize the doses of compounds for senescence induction, we tested different concentrations of the compounds and chose the doses that did not induce substantial cell death (Figure 2A and Supplemental Figure S1F). Cells were exposed to these compounds for 4 d (d4), followed by a further incubation without the compounds for 5 d (d9) to examine the phenotype irreversibility, a critical feature of senescence.

We confirmed that the majority of IRG-treated cells exhibited enlarged and irregular-shaped nuclei after a 4-d treatment and these nuclear phenotypes were maintained after the compounds

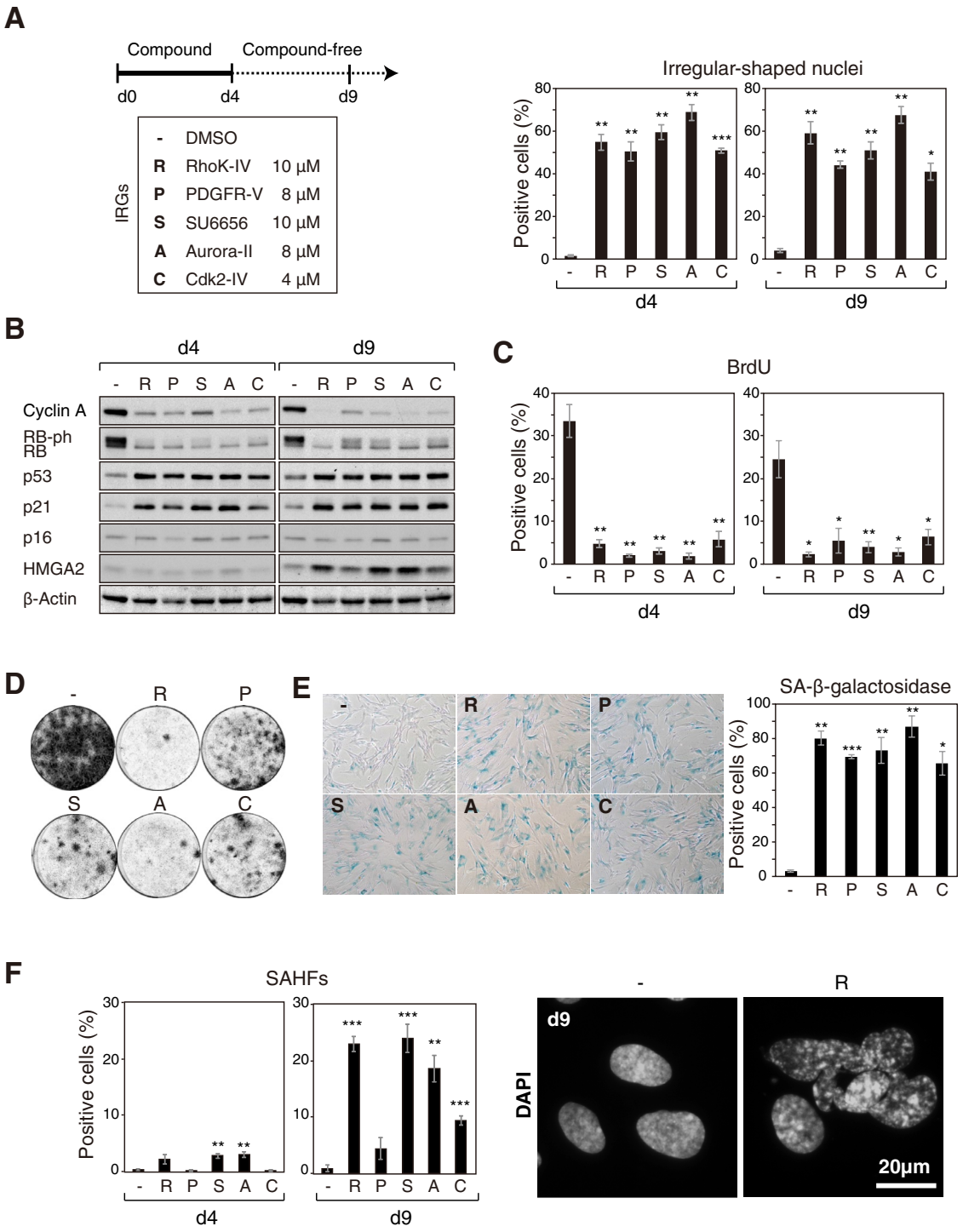

FIGURE 2: "Irregular-shaped" nuclear phenotype is associated with cellular senescence. (A) IMR90 cells were exposed to the hit compounds that induce formation of the irregular-shaped nuclei (IRGs) for 4 d (d4), followed by a 5-d incubation in compound-free medium (d9). The percentage of cells showing irregular-shaped nuclei at the indicated time points was assessed using DAPI staining. (B) Immunoblot analysis for the indicated proteins. RB-ph, phosphorylated RB. (C) Percentage of BrdU incorporation–positive cells. (D) For colony formation assay, cells were plated without compounds after a 4-d treatment with IRGs. (E) SA-β-gal activity in the compound-free cells (d9). (F) Cells indicated were assessed for SAHF formation. Values are mean ± SEM from three independent experiments. *$p < 0.05$, **$p < 0.01$, ***$p < 0.001$.

had been removed (Figure 2A and Supplemental Figure S2). IRGs also induced a stable cell cycle arrest, as determined by a reduction in cyclin A, the phosphorylation status of RB (Figure 2B), and 5-bromo-2′-deoxyuridine (BrdU) incorporation (Figure 2C), even after compound removal. Consistently, the number of colony-forming cells after 2-wk incubation with compound-free medium was strongly reduced if they were pretreated with IRGs (Figure 2D), reinforcing the long-term nature of the observed cell cycle arrest. To further confirm that the IRGs induce senescence, we measured SA-β-gal activity, a hallmark of senescence (Dimri *et al.*, 1995). Cells

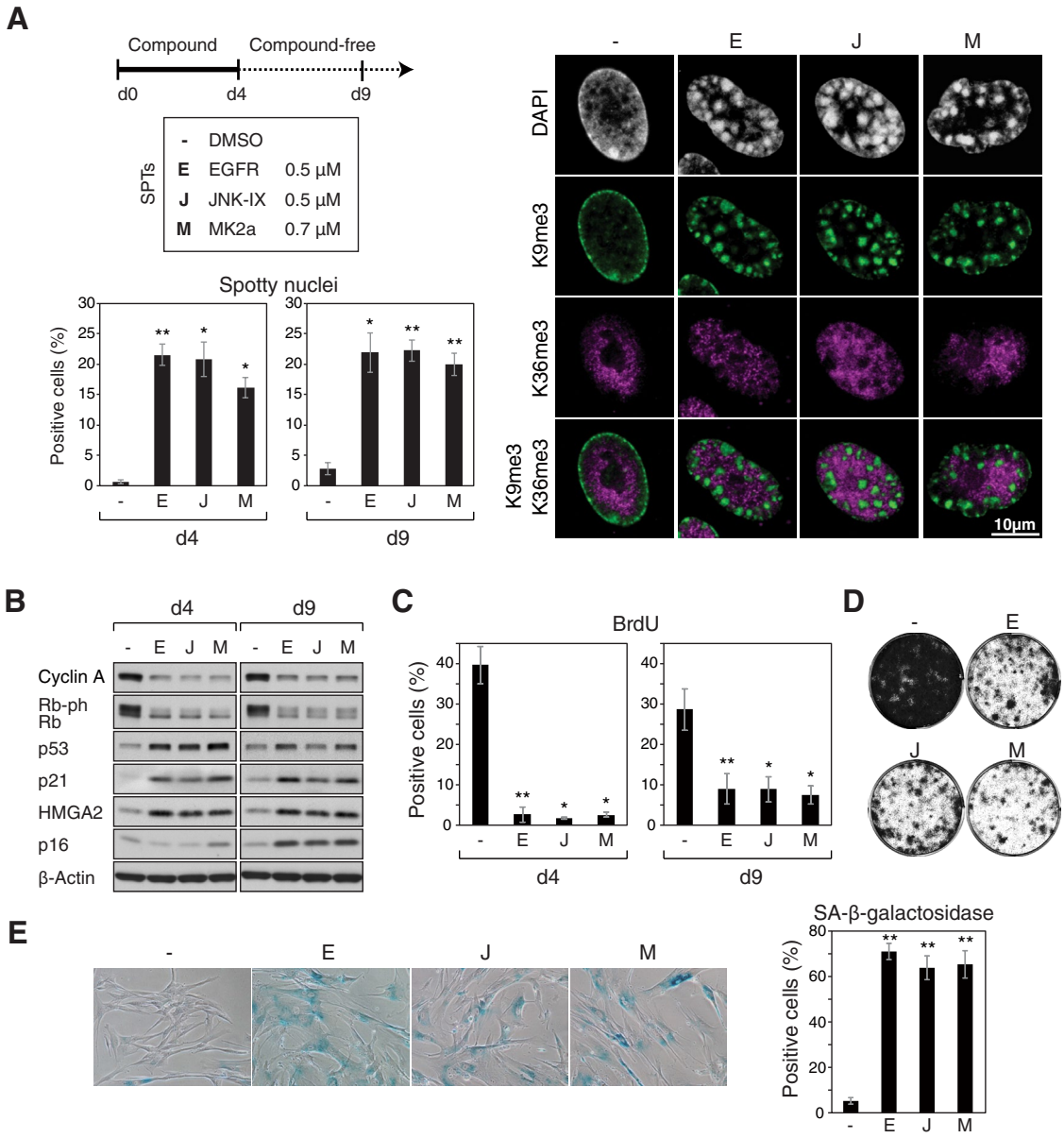

FIGURE 3: "Spotty" nuclear phenotype is associated with cellular senescence. (A) Cells were assessed for formation of a spotty nucleus using immunofluorescence. Right, confocal images of the cells immunostained for histone H3 trimethylated at lysine 9 (H3K9me3) and H3K36me3, markers of heterochromatin and euchromatin, respectively, and counterstained with DAPI. DAPI foci were colocalized with H3K9me3. (B) Immunoblot analysis in the compound-treated cells using the indicated antibodies. (C) Percentage of BrdU incorporation–positive cells. (D) After a 4-d treatment with the SPTs, cells were plated without the compounds in equal number for the colony formation assays. (E) SA-β-gal activities in the indicated cells at d9.*$p < 0.05$, **$p < 0.01$.

pretreated with the IRGs typically showed an enlarged cellular morphology with increased SA-β-gal activity (Figure 2E). Although the levels of p16, a senescence-associated CDK inhibitor, were unaltered, p53 and its target p21 (another CDK inhibitor), both of which play important roles in senescence in some contexts (Chang *et al.*, 2000, 2002), were stably upregulated in IRG-treated cells (Figure 2B). Of interest, the levels of HMGA2, a senescence marker associated with SAHFs (Funayama *et al.*, 2006; Narita *et al.*, 2006), were increased only at the later time point. Consistently, SAHF formation was also more evident at d9 (Figure 2F), and thus senescence is progressively established even during the compound-free period. These results suggest that senescence is not an immediate outcome of the treatment but rather a delayed phenotype. Consistent with recent reports that demonstrated a senescence-associated lamin B1 reduction (Shimi *et al.*, 2011; Salama *et al.*, 2014), lamin B1 was down-regulated in IRG-treated cells (Supplemental Figure S3, A and B). Of note, induction of the irregular nuclear shape in IRG-treated cells preceded lamin B1 reduction (Supplemental Figure S3C), suggesting that the lamin B1 reduction is not the cause of the irregular nuclei. These compounds also induced senescence in BJ cells (another HDF), although some compounds induced a milder phenotype than in IMR90 cells (Supplemental Figure S4).

Similarly to IRGs, we also tested selected SPT hits in the secondary senescence assays. These compounds were more toxic than the IRGs, and we used a lower concentration for our validation experiments. At the concentrations used (Figure 3A), the viability of cells

24 h after drug treatment was >90% (Supplemental Figure S1F). Although the nuclear phenotype was relatively modest compared with the IRG hits, the formation of DAPI foci was significantly increased after treatment with the SPT hit compounds (Figure 3A). These foci were colocalized with H3K9me3 but excluded H3K36me3 and are thus morphologically similar to SAHFs. Consistently, p21 and p16, which have been shown to be effectors of SAHF formation, were both up-regulated (Figure 3B). Cells pretreated with these compounds were stably arrested and displayed additional features of senescence (Figure 3, B–E). Together our data provide a proof of principle that the nuclear phenotypes can be used as a readout for prosenescence screens. For further validation of the compounds and nuclear phenotypes in the context of senescence in this study, we decided to focus on IRGs and their associated phenotype, which were strong and highly distinctive.

IRG compounds induce premature exit from M phase and tetraploidization

To examine at which cell cycle stage the IRG-treated cells accumulate and become senescent, we analyzed cell cycle profiles and the expression pattern of cyclins by laser scanning cytometer and immunoblotting, respectively. After treatment with IRGs, the number of cells with a 4*n* DNA content became markedly increased compared with mock-treated cells (Figure 4A). In addition there was an increase in the number of cells with an 8*n* DNA content. Of interest, immunoblot analysis showed that those cyclins enriched in G2 or M phase (cyclin A or B1, respectively) were decreased, whereas a G1 cyclin (cyclin D1) was increased during IRG-induced senescence (Figure 4B). These data suggest that the increased 4*n* DNA content reflects cell cycle arrest in G1 phase after a failed mitosis (i.e., a tetraploid state) rather than G2 arrest. This is highly reminiscent of Aurora kinase B (AURKB) inhibitors, which induce irregular-shaped nuclear formation with polyploidization (Ditchfield *et al.*, 2003; Hauf *et al.*, 2003). Indeed, the IRGs included some compounds (Aurora kinase inhibitor II and SU6656) that can inhibit AURK (Bain *et al.*, 2007). Therefore we tested whether the inhibition of AURKB activity by ZM1 (ZM447439; Girdler *et al.*, 2006), a well-established AURKB inhibitor, causes cellular senescence in HDFs. Treatment of both IMR90 and BJ cells with ZM1 phenocopied the IRG effect. Consistent with the previous studies, ZM1 treatment induced tetraploidy with a highly irregular nuclear shape (Figure 4, A–C). Detailed senescence assays confirmed that ZM1-pretreated cells exhibited a stable exit from the cell cycle with increased senescence markers (Figure 4C). Similar to cells exposed to IRG compounds, ZM1-treated cells ceased to proliferate by d4, at which point they had irregular nuclei and were mostly tetraploid. However, the establishment of senescence again appeared to be delayed, steadily developing beyond the 4d treatment (Figure 4C; see SAHF count and HMGA2 blotting). Similar results were obtained using AZD1152, another specific inhibitor of AURKB (Wilkinson *et al.*, 2007; Supplemental Figure S5). Together these data suggest that IRG compounds may induce senescence at least in part by directly or indirectly inhibiting AURKB activity.

To confirm directly the correlation between irregular nuclei and tetraploidy, we tracked the fate of mitotic nuclei by live-cell imaging of cells expressing H2B:enhanced yellow fluorescent protein (EYFP) that had been treated with the compounds. As shown in Figure 4D, cells treated with the compounds entered M phase and condensed their chromosomes, yet they eventually decondensed without proper segregation and formed mostly single and irregular-shaped nuclei (Figure 4D, Supplemental Movies S1–S3, and Supplemental Table S4). These data suggest that the irregular-shaped nuclei arise immediately after M phase without proper chromosome segregation and that cell cycle arrest at the G1 tetraploid phase is maintained during senescence development in normal HDFs.

Premature exit from M phase without chromosome segregation takes place after prolonged mitosis (mitotic slippage; Gascoigne and Taylor, 2009) or when the spindle checkpoint is restrained (Vitale *et al.*, 2011). Inhibition of microtubule dynamics by paclitaxel (Taxol; a microtubule-stabilizing agent) activates the mitotic checkpoint to keep cells arrested at the metaphase/anaphase boundary, at which the well-known mitosis marker histone H3 phosphorylated at serine 10 (H3S10ph), a direct substrate of AURKB and cyclin B, accumulates (Figure 4E, lane 2). It has been shown that treatment with AURKB inhibitors overrides the paclitaxel-induced SAC (Ditchfield *et al.*, 2003; Hauf *et al.*, 2003). To test whether treatment with the IRGs also cancels the paclitaxel-induced SAC, we synchronized IMR90 cells with paclitaxel treatment for 12 h and then released cells into paclitaxel with or without IRGs or ZM1 (Figure 4E). Similar to ZM1 (Figure 4E, lane 9), the paclitaxel-induced checkpoint was rapidly canceled by the addition of each of the IRGs (Figure 4E, lanes 4–8), whereas accumulation of cyclin B1 and H3S10ph was virtually unaffected by the treatment with SPTs (Supplemental Figure S6, lanes 10–12). These results further support our hypothesis that treatment with IRGs induces the irregular nuclear phenotype with tetraploidization through AURKB inhibition.

It has been shown that AURKB inhibition does not have a substantial effect on the viability of nonproliferating cells (Ditchfield *et al.*, 2003; Hardwicke *et al.*, 2009). To study whether cell cycle progression is required for IRGs to induce senescence, we treated quiescent IMR90 cells, induced by serum starvation, with the compounds for 3 d (Supplemental Figure S7A). We then released the compound-treated cells from quiescent arrest into compound-free normal medium (10% serum). The pretreated cells (during quiescence) failed to change their nuclear morphology (Supplemental Figure S7, A and B) and exhibited virtually no reduction in their proliferative capacity (Supplemental Figure S7C). Therefore IRGs and ZM1 induce senescence in proliferating but not in nonproliferating cells. Together these results suggest that, although these compounds have multiple targets, the downstream effects may converge on AURKB, which appears to be the dominant pathway for their senescence-inducing activity.

Specific inhibition of Aurora B kinase activity triggers formation of irregular-shaped nuclei and cellular senescence

We next tested whether the IRGs directly inhibit AURKB kinase activity, using a biochemical kinase profiling assay. Consistent with the phenotypic similarity between IRGs and ZM1 treatment, all five IRGs exhibited a substantial inhibitory effect against AURKA and AURKB, with stronger effects on AURKB, whereas the SPT hits showed virtually no effect on the activities of the AURKs (Figure 5A). Although ZM1-induced polyploidization has been attributed to AURKB inhibition (Ditchfield *et al.*, 2003; Hauf *et al.*, 2003; Girdler *et al.*, 2006), ZM1 also inhibits AURKA, which has both a very distinct localization pattern and functions differently from AURKB, and, in addition to the AURKs, IRGs have multiple targets.

To suppress specifically AURKB activity, we next sought to apply either a stable RNA interference (RNAi) or a dominant-negative approach. Using a microRNA (miR30)-based design (Silva *et al.*, 2005), we identified at least two *sh-AURKB* constructs that substantially down-regulated the endogenous levels of AURKB and induced comparable phenotypes in IMR90 cells when stably transduced (Supplemental Figure S8). We also generated retroviral constructs encoding either an enhanced green fluorescent protein (EGFP)–tagged

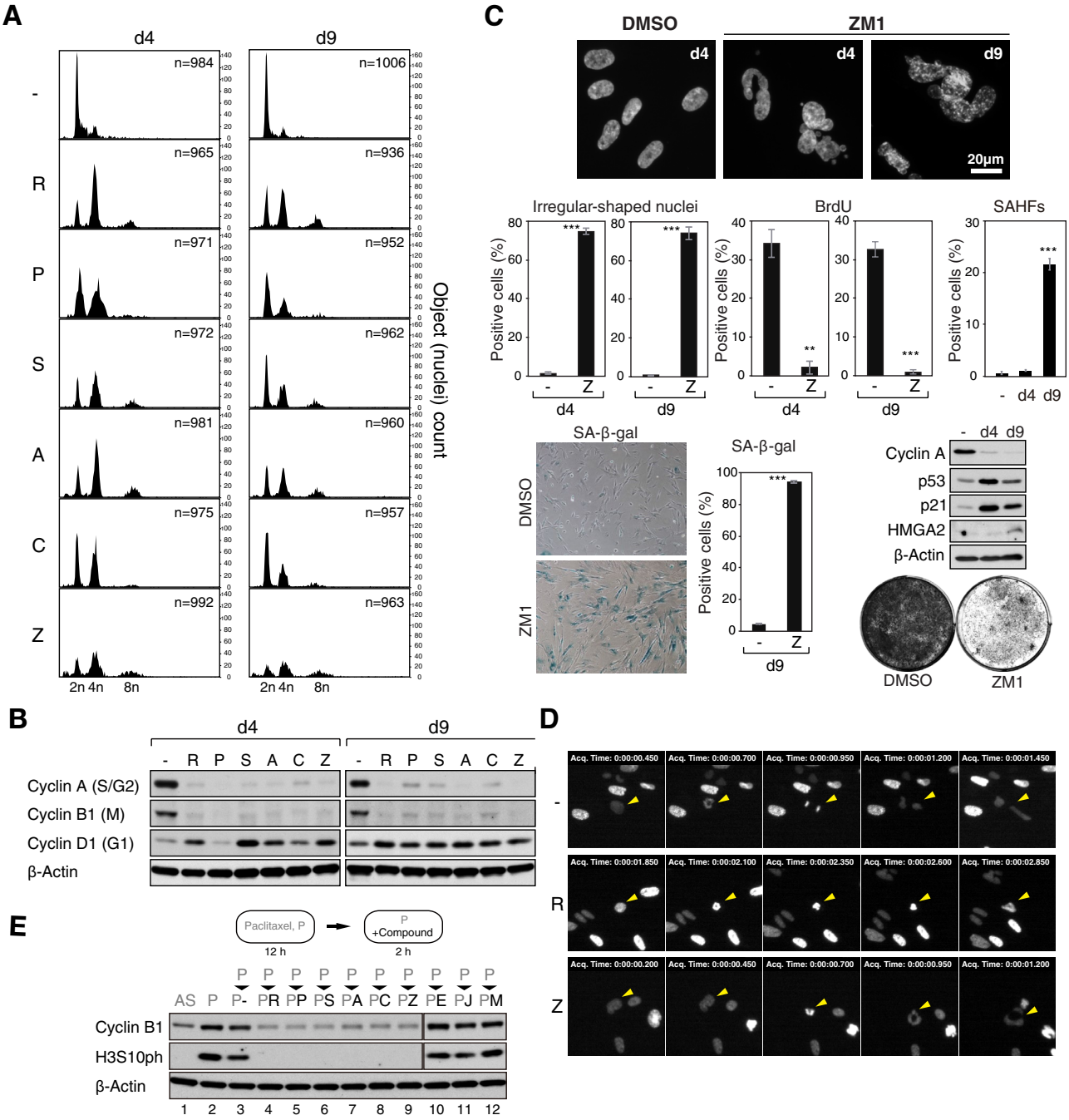

FIGURE 4: Aurora kinase inhibition phenocopies IRG treatment in IMR90 cells (A) Cell cycle profiles of the cells treated as in Figure 2A were analyzed by laser scanning cytometry. In addition to IRG hits, the AURKB inhibitor ZM1 (2 μM; Z) was included. (B) Accumulation of a G1-phase cyclin in the IRG- or ZM1-treated cells. (C) ZM1 treatment induces senescence in IMR90 cells. Cells treated as in A were assessed for nuclear morphology, BrdU incorporation, SAHF formation, SA-β-gal activities, expression of indicated proteins, and colony formation. $^{**}p < 0.01$, $^{***}p < 0.001$. (D) Time-lapse images of the nuclei in compound-treated cells expressing H2B-EYFP (see Supplemental Movies S1–S3). Compounds were added when the cells were released from G1/S, and the first mitoses were recorded. (E) Treatment of cells with IRGs elicits exit from paclitaxel-induced M-phase arrest. IMR90 cells were synchronized in M phase by paclitaxel (P) for 12 h, and the indicated hit compounds were added and incubated for 2 h. For comparison, we also used the spotty hit compounds, which failed to induce a premature exit from the paclitaxel-induced M-phase arrest (lanes 10–12 [see Supplemental Figure S6]). M-phase cells were assessed using the levels of cyclin B1 and histone H3 phosphorylation at serine 10 (H3S10ph; a direct substrate of AURKB). The blots for cyclin B1 and H3S10ph in the paclitaxel-treated cells (left) were run in the same gel (see full lanes in Supplemental Figure S6).

wild-type or a kinase-dead AURKB mutant ($AURKB^{D218N}$), which was previously shown to function in a dominant-negative manner (Girdler *et al.*, 2006). Endogenous AURKB levels were also down-regulated in cells expressing $AURKB^{D218N}$ or treated with ZM1 (Figure 5B), perhaps due to the cell cycle arrest in the tetraploid G1 phase caused by AURKB inhibition (Gully *et al.*, 2012). Immunoblot analysis showed

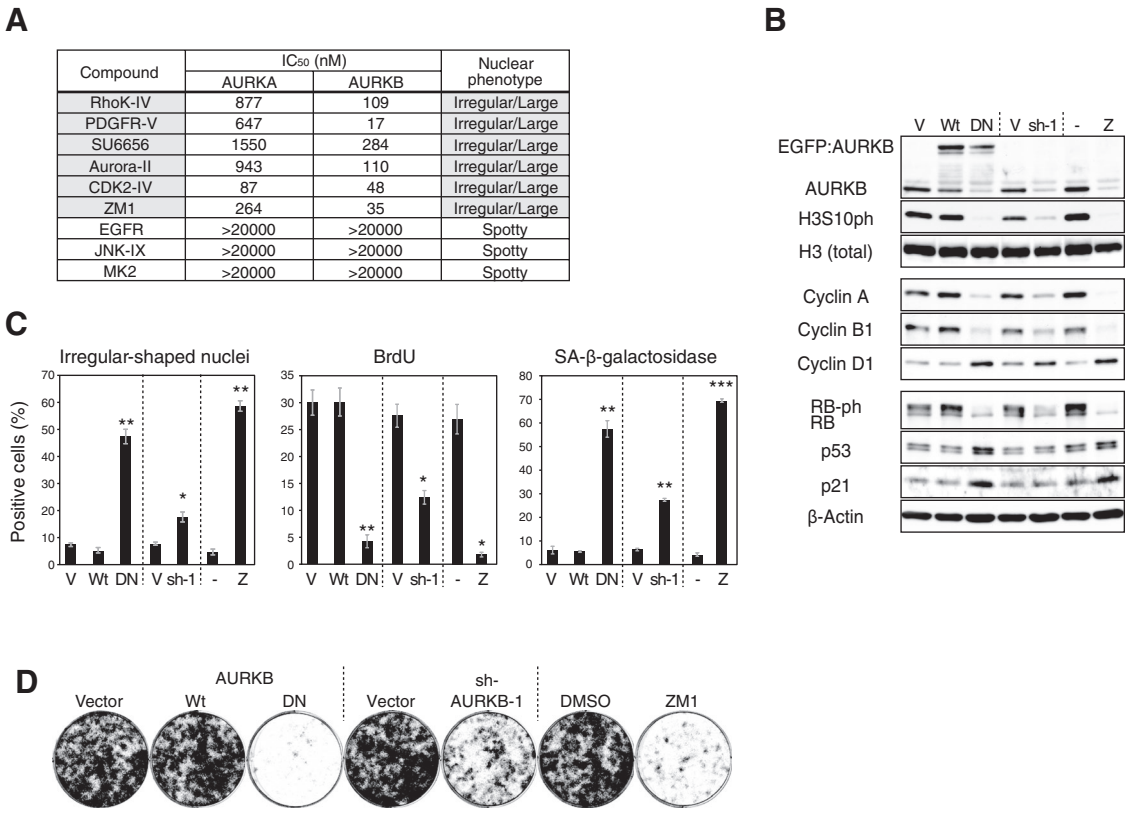

Compound	IC_{50} (nM)		Nuclear phenotype
	AURKA	AURKB	
RhoK-IV	877	109	Irregular/Large
PDGFR-V	647	17	Irregular/Large
SU6656	1550	284	Irregular/Large
Aurora-II	943	110	Irregular/Large
CDK2-IV	87	48	Irregular/Large
ZM1	264	35	Irregular/Large
EGFR	>20000	>20000	Spotty
JNK-IX	>20000	>20000	Spotty
MK2	>20000	>20000	Spotty

FIGURE 5: Specific inhibition of Aurora B kinase activity induces cellular senescence. (A) In vitro kinase activity assay. The IC_{50} of the indicated compounds was determined using an in vitro kinase activity assay for AURKA or AURKB. (B–D) Genetic inhibition of AURKB activity induces cellular senescence. IMR90 cells were stably transduced with retroviral vectors expressing EGFP-tagged wild-type (Wt) or kinase-dead dominant-negative (DN) mutant ($AURKB^{D218N}$) AURKB, sh-AURKB-1 (sh-1; Supplemental Figure S8), or corresponding controls (V; EGFP or miR30 vector, respectively). Cells were also treated with ZM1 (Z) or DMSO (–) for comparison (d9). At d6 after retroviral infection and selection, cells were assessed for protein expression (B) and irregular-shaped nuclei, BrdU incorporation, and SA-β-gal activity (C). Values are mean ± SEM from three independent experiments. *$p < 0.05$, **$p < 0.01$, ***$p < 0.001$. Cells were also plated at the same density and assessed for colony formation (D).

that expression of $AURKB^{D218N}$ or *sh-AURKB-1* or ZM1 treatment resulted in a reduction in H3S10ph (Figure 5B). Cyclin A, cyclin B1, and phosphorylated RB were down-regulated, whereas cyclin D1 (a G1 cyclin) was increased in $AURKB^{D218N}$- or *sh-AURKB-1*–expressing cells, as observed in IRGs/ZM1-treated cells (Figure 5B; also Figure 4B). The nuclear phenotype with irregular shape was comparable between $AURKB^{D218N}$-expressing cells and ZM1-treated cells, whereas *sh-AURKB-1*–expressing cells showed a milder phenotype (Figure 5C). Consistently, the senescence phenotype was also milder in the *sh-AURKB-1*–expressing cells (Figure 5, B–D). Of note, cells expressing *sh-AURKB-1* exhibited residual H3S10ph (Figure 5B), and thus the milder phenotype of *sh-AURKB-1*–expressing cells might be due to a residual activity of AURKB (see also Supplemental Figure S8, A and B, for a dose-dependent correlation between AUKB1 levels and proliferative arrest). Together these results indicate that AURKB inhibition–induced senescence progressively develops in tetraploid cells with a highly irregular nuclear morphology and is an immediate consequence of AURKB inhibition in normal HDFs.

Knockdown of p53 partially rescues IRG-induced senescence in IMR90 cells

We next tested whether IRG-induced senescence is dependent on p53 in IMR90 cells, using a miR30 design–based RNAi-mediated knockdown of p53 (Figure 6A; Kirschner *et al.*, 2015). AURKB inhibition induced irregular-shaped nuclei at a similar frequency in both control and sh-p53–expressing cells (Figure 6, B and C). However, the nuclear phenotype of the sh-p53–expressing cells was highly heterogeneous, and nuclear enlargement was more pronounced than in control cells (Figure 6, B and E). Reduction of BrdU incorporation was partially rescued by p53 depletion, with a corresponding increase in the polyploid population (Figure 6, C and D). These results are consistent with previous studies suggesting that deficiencies in the p53-p21 pathway enhance the endoreduplication caused by Aurora kinase inhibitors (Ditchfield *et al.*, 2003; Gizatullin *et al.*, 2006; Kaestner *et al.*, 2009). Accumulation of SA-β-gal activity and reduced long-term proliferative capacity were also partially rescued by p53 knockdown (Figure 6, F and G). These results suggest that p53 is not required for the irregular nuclear phenotype but that the overall senescence phenotype is partially dependent on p53.

IRG compounds block the proliferation of cancer cells

AURKB inhibition in tumor cells leads to increased polyploidy and cell cycle arrest or cell death, depending on the cell type or context (Ditchfield *et al.*, 2003; Hauf *et al.*, 2003; Gizatullin *et al.*, 2006; Wilkinson *et al.*, 2007; Yang *et al.*, 2007). For example, in the presence of AURKB inhibitors, HeLa cervical carcinoma cells enter and exit mitosis normally but fail to divide (Ditchfield *et al.*, 2003; Hauf *et al.*, 2003). However, long-term senescence development in tumor

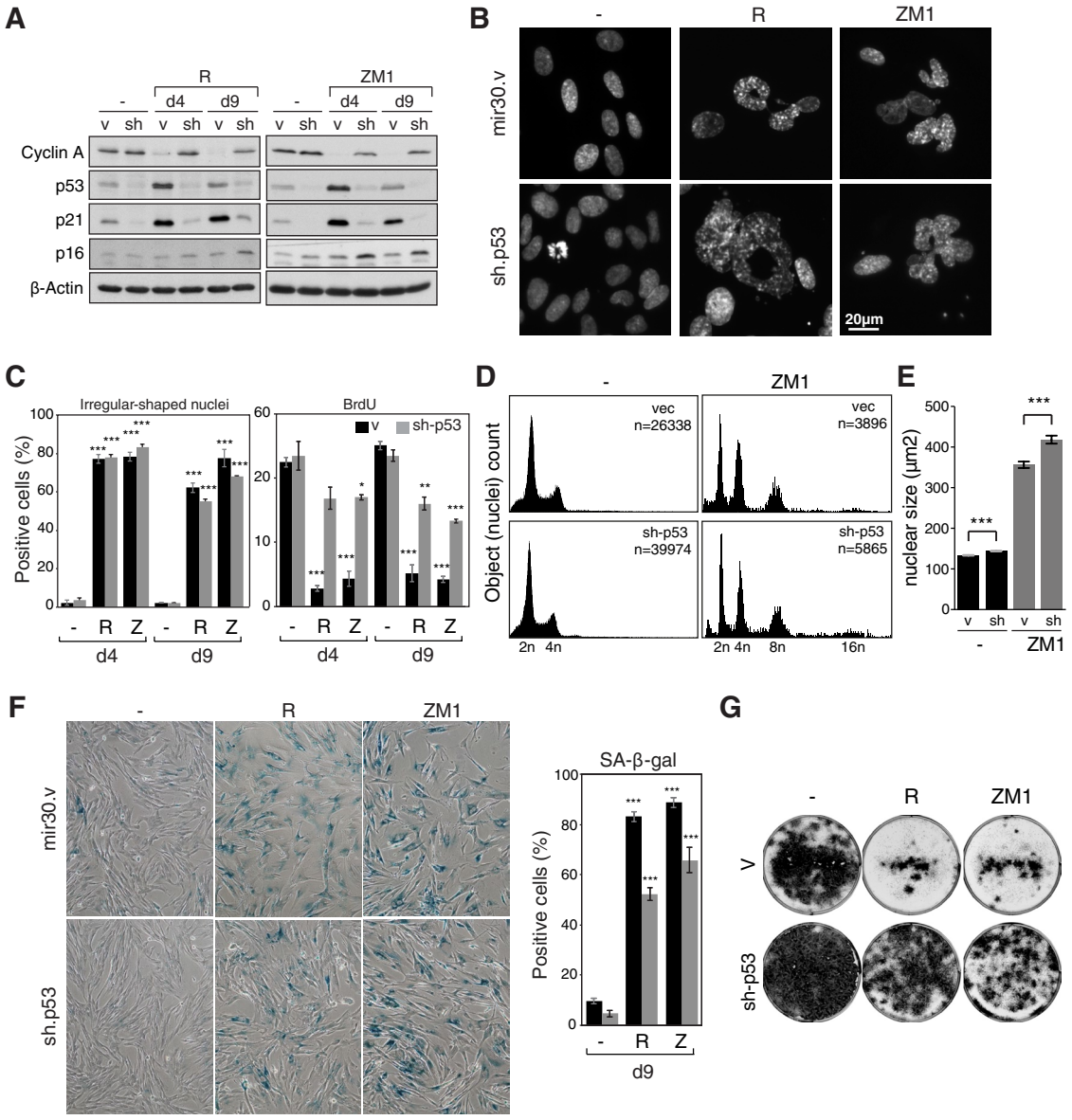

FIGURE 6: Effect of p53 knockdown on IRG compound–induced senescence in IMR90 cells. (A) Immunoblot analysis for the indicated proteins in cells expressing sh-p53 or control vector, which were treated with RhoK-IV (R), ZM1, or DMSO (–) for 4 d (d4), followed by a 5-d culture in compound-free medium (d9). (B) Fluorescence (DAPI) images of the indicated cells treated as in A at d9. (C) Percentage of indicated cells with irregular-shaped nuclei or BrdU incorporation at the indicated time points. R, RhoK-IV; Z, ZM1; –, DMSO. Values are the mean ± SEM from three independent experiments. *$p < 0.05$, **$p < 0.01$, ***$p < 0.001$. (D, E) Cell cycle profiles (D) and nuclear area size (E) of the indicated cells treated as in A were analyzed by laser scanning cytometry at d9. (F) SA-β-gal activity in the indicated cells at d9. Values are the mean ± SEM from three independent experiments. ***$p < 0.001$. (G) Colony formation assays for the indicated cells pretreated with the indicated compounds for 4 d.

cells pretreated with AURK inhibitors remains to be determined. To test whether these compounds cause TIS in tumor cells, we treated HeLa cells with selective IRGs as well as ZM1. We first confirmed that cells were mostly viable (~80% at day 9; Supplemental Figure S9A) after treatment with the compounds at the concentrations used. Consistent with the phenotype of AURKB inhibition, after a 4-d treatment with these compounds, the cells contained remarkably enlarged and highly irregular/multilobulated nuclei or often had numerous nuclei per cell (Figure 7A). At this stage, the cells showed only a modest retardation of cell cycle progression with little sign of senescence (probed through phosphorylation status of RB and BrdU incorporation; Figure 7, B and C). After an additional 5-d incubation in compound-free medium, however, cells exhibited an accumulation of the G1 cyclin (cyclin D1) and reduced markers of cell cycle progression, such as the S/G2 cyclin (cyclin A), phosphorylated forms of RB, and BrdU incorporation (Figure 7, B and C), suggesting that the compound-pretreated cells eventually arrest at a polyploid G1 phase. These cells also showed a robust accumulation of SA-β-gal activity (Figure 7, D and E). Thus the IRG compounds can induce senescence in HeLa cells. Their long-term arrest was confirmed using colony formation assays in compound-free medium (Figure 7F). Of interest, we found that the p53-p21 pathway and HMGA2 were up-regulated, particularly at d9 (Figure 7B). Note, however, that in HeLa cells, the level of wild-type endogenous p53

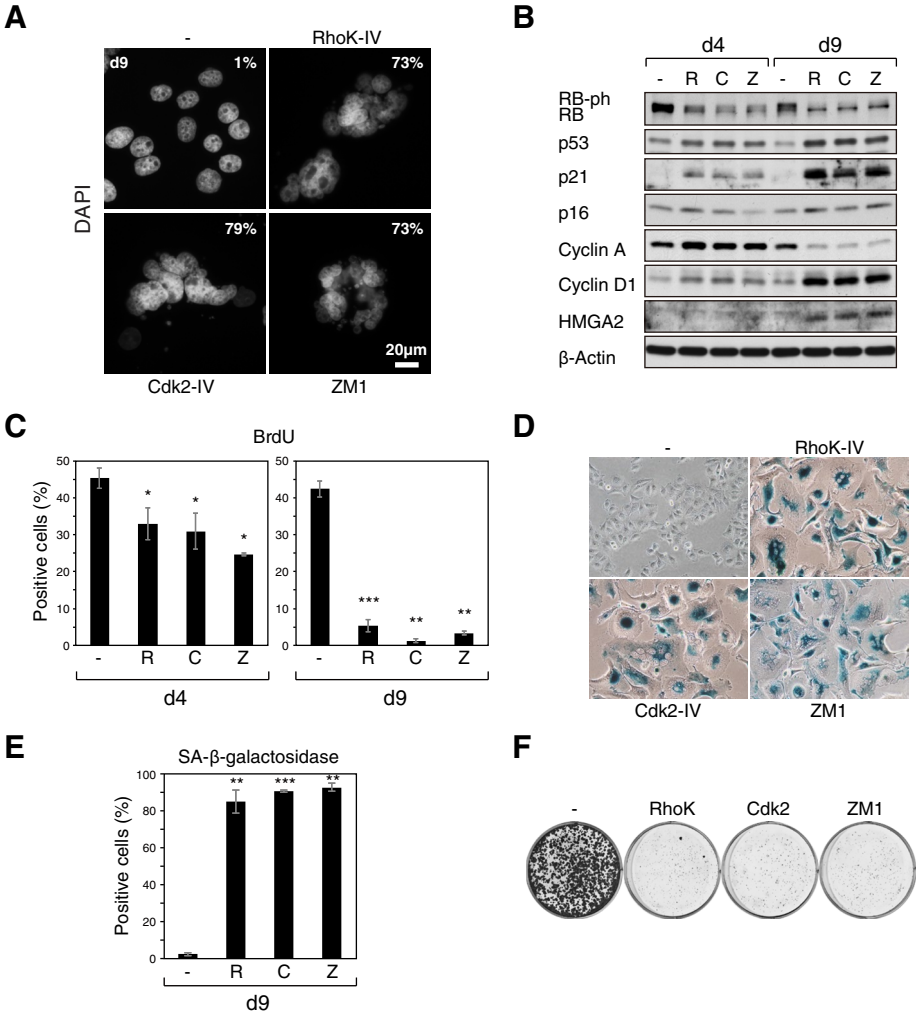

FIGURE 7: HeLa cells undergo cellular senescence by treatment with IRGs. (A) Fluorescence (DAPI) images of HeLa cells treated with selected IRG compounds and ZM1 for 4 d, followed by a 5-d culture in compound-free medium (d9) as in Figure 2A. RhoK-IV, Cdk2-IV, and ZM1 were used at 1.5, 4, and 1.5 μM, respectively. DNA was stained with DAPI. Numbers represent percentages of nuclei with an irregular shape (d9). (B) Immunoblot analysis for the indicated proteins in HeLa cells at d4 and d9. (C) Percentage of cells that are BrdU incorporation positive. (D, E) SA-β-gal assays for the compound-pretreated HeLa cells at d9; representative images (D) and quantitative data (E). *$p < 0.05$, **$p < 0.01$, ***$p < 0.001$. (F) Colony formation assays in HeLa cells pretreated with indicated compounds for 4 d. Values are mean ± SEM from three independent experiments.

is suppressed by human papillomavirus E6, it has been shown that p53 can escape from its E6-mediated down-regulation upon stress in some contexts (Wesierska-Gadek *et al.*, 2002; Li and Anderson, 2014), and our data suggest that treatment with these compounds is also able to restore endogenous p53 levels in the presence of E6 as a long-term effect, further reinforcing the progressive nature of senescence establishment after removal of the compounds.

We next asked whether these compounds induce senescence in tumor cells that completely lack p53, using H1299, a p53-null human lung cancer cell line. Although some rounded-up or floating cells were observed at both d4 and d9, IRG-treated H1299 cells were largely viable (Supplemental Figure S9B). Similar to HeLa cells, the cells that were attached exhibited highly enlarged irregular/lobulated nuclei and/or a multinuclear phenotype (Figure 8A), the progressive accumulation of G1 cyclin (cyclin D1) (Figure 8B), and a significant reduction in BrdU incorporation (Figure 8C), suggesting that the IRG/ZM1-pretreated cells also develop the G1 polyploid phenotype. Although the reduction in DNA synthesis and cyclin A levels was less pronounced than in HeLa cells at d9, the pretreated H1299 cells showed a strong senescence-like phenotype (Figure 8D) with a marked reduction in their colony-forming capacity, likely due to a combination of senescence and cell death (Figure 8E). Of interest, p21 up-regulation was observed at later time points in H1299 cells, suggesting the existence of a p53-independent mechanism for p21 induction in this context (Figure 8B; Macleod *et al.*, 1995). Taken together, our data suggest that AURKB inhibition triggers senescence and that this senescence develops while the cells are in a tetraploid state or, in the case of the tumor cells with reduced or defective p53, a polyploid state.

DISCUSSION

Although the primary endpoint of conventional chemotherapy is generally cell death, senescence is gaining increasing attention as an alternative goal in cancer therapy (Acosta and Gil, 2012; Cairney *et al.*, 2012). Senescence is a heterogeneous and collective phenotype mediated by multiple effector programs, which are often associated with distinct senescence markers (Salama *et al.*, 2014). This predicts the benefit of using diverse markers as readouts in screens for senescence inducers and/or senescence bypass. Here we focus on nuclear/chromatin morphological alterations, allowing us to identify multiple compounds that induce "tetraploid senescence," likely through a direct inhibition of AURKB in a progressive manner. Indeed, a small 8*n* cell population can be seen in conventional RAS-induced senescent cells (Supplemental Figure S1), suggesting that our screen simply captured an enrichment of certain subtypes of the senescence phenotype. Of importance, such a system of "high-content" analyses could be extended through additional readouts and also allows for flexible strategies, which could be targeted at broader, or tuned for specific, senescence effector programs. Although, as a proof of principle, we used normal HDFs, which are highly prone to senescence, and a kinase inhibitor library with a modest specificity and diversity (160 inhibitors), some of the hits were capable of inducing senescence in tumor cell lines. Thus the system is potentially applicable to TIS screening, with higher throughput and/or different types of libraries. Although our data indicate that IRGs induce senescence through AUKB inhibition, it is important to note that additional "on-target" effects of such multitarget inhibitors might confer additional effects on and/or modulate their AURKB inhibitory activity.

The Aurora kinases are overexpressed in a wide range of human cancers and are considered as promising therapeutic targets, and a number of clinical trials are at various stages (Keen and Taylor, 2004; Green *et al.*, 2011; Goldenson and Crispino, 2015). These studies

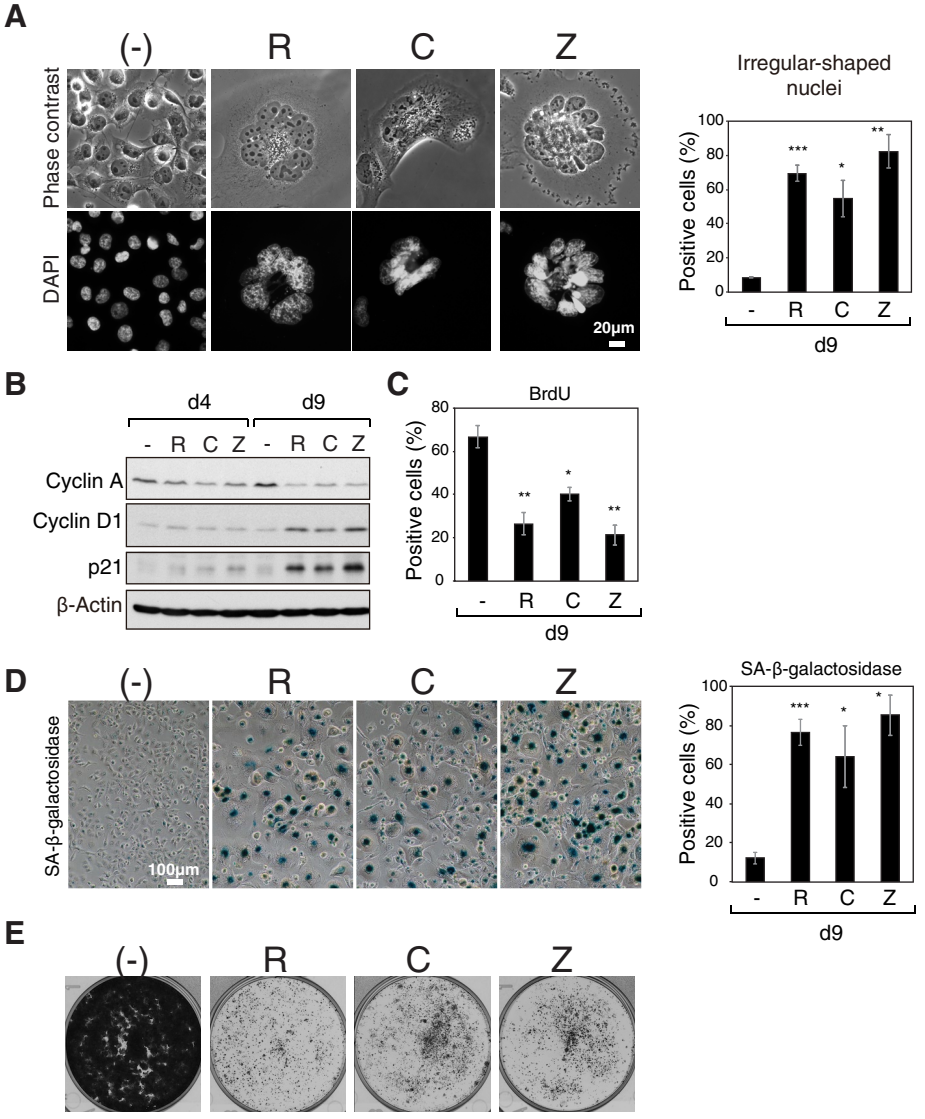

FIGURE 8: p53-null cancer cells undergo cellular senescence by treatment with IRGs. (A) Phase contrast and DAPI images of H1299 cells treated with selected IRG compounds and ZM1 for 4 d, followed by a 5-d culture in compound-free medium (d9) as in Figure 2A. (B) Immunoblot analysis for the indicated proteins in H1299 cells at d4 and d9. (C) Percentage of the BrdU incorporation–positive cells. (D) SA-β-gal assays for the compound-pretreated H1299 cells at d9; representative images (D) and quantitative data (E). Values are mean ± SEM from three independent experiments. *$p < 0.05$, **$p < 0.01$, ***$p < 0.001$. (E) H1299 cells pretreated with the indicated compounds for 4 d were maintained in normal media for colony formation assay.

are aimed at inducing cell death, and the induction of a senescence-like response has not been considered in these trials.

Inhibition of AURKB overrides the SAC, thereby inducing a premature exit from mitosis and interfering with cytokinesis, leading to tetraploid/binuclear cells (Keen and Taylor, 2009). However, how AURKB inhibition develops into a senescence phenotype in the tetraploid condition remains to be elucidated. Tetraploidization can also be induced by mitotic slippage after a prolonged mitosis, cytokinesis failure, endoreduplication, telomere dysfunction, DNA-damaging agents, or cell fusion (Storchova and Kuffer, 2008; Davoli *et al.*, 2010; Davoli and de Lange, 2011; Johmura *et al.*, 2014; Panopoulos *et al.*, 2014). In addition, it was recently shown that "mitotic skip" is involved in tetraploid senescence, particularly when induced by DNA damage, in which p53 activation during G2 plays a key role, although possible functional relation between tetraploidization and senescence was not examined (Johmura *et al.*, 2014; Krenning *et al.*, 2014).

Tetraploid cells are suggested to be genetically unstable and have a risk of producing aneuploidy, a hallmark of cancer cells (Fujiwara *et al.*, 2005; Ganem *et al.*, 2007; Storchova and Kuffer, 2008; Davoli *et al.*, 2010). It has been controversial whether a p53-dependent G1 "tetraploidy checkpoint," which senses an excessive number of chromosomes or centrosomes, exists (Andreassen *et al.*, 2001; Margolis *et al.*, 2003; Uetake and Sluder, 2004; Wong and Stearns, 2005; Hayashi and Karlseder, 2013). Of interest, however, Ganem *et al.* (2014) recently showed that tetraploidization can trigger a "G1 arrest" without an apparent DNA-damage response, through the activation of the Hippo and p53 pathways. It would be very interesting to test whether AURKB inhibition-induced senescence is, at least in part, dependent on these pathways.

Our data suggest that senescence is a delayed process rather than an immediate consequence of tetraploidization. Although a polyploid chromosome number might contribute to inducing senescence by itself, it is also possible that the pathophysiology behind polyploidization could progressively provoke senescence effector mechanisms. Indeed, both senescence and tetraploidy are associated with some common pathophysiological contexts, including wound healing, aging, preneoplasia, and embryonic development (Ermis *et al.*, 1998; Ganem *et al.*, 2007; Davoli and de Lange, 2011; Gentric *et al.*, 2012; Chuprin *et al.*, 2013). Although the p53-defective cells treated with the AURKB inhibitor underwent substantial endoreduplication and became highly polyploid, we saw only a partial progression to senescence in these cells (Figures 6–8), and some senescence escape was observed, particularly in normal cells (Figure 6). However, it remains unclear whether, in p53-defective conditions, a small fraction of the cells that escaped from the initial mitotic defect eventually grew out or whether some polyploid senescent cells resumed a normal cell cycle.

Persistent senescent cells in vivo may contribute to tumorigenesis through the SASP, particularly in TIS conditions (Coppé *et al.*, 2010; Jackson *et al.*, 2012; Dörr *et al.*, 2013). Of interest, typical SASP factors, including MMP3, IL6, and IL8 were not induced in AURKB inhibition–induced senescent cells (Supplemental Figure S10). Although more detailed analyses would be required, our data suggest that AURKB inhibition might provide a unique therapeutic opportunity, which alleviates the non–cell-autonomous tumorigenic effects of senescence. Of note, the SASP is also involved in the immune-mediated elimination of senescent cells (Xue *et al.*, 2007; Kang *et al.*, 2011), and without this step, "unstable" senescent cells

may recur (Kang *et al.*, 2011). Of interest, the fate of senescence "escapers" has been linked to "mitotic catastrophe," a distinct form of cell death that occurs soon after mitotic failure by poorly understood mechanisms (Shay and Wright, 2005; Vitale *et al.*, 2011; Hayashi and Karlseder, 2013). The mitotic catastrophe and cell death after senescence escape have also been associated with deficiencies in the p53-p21 pathway in tumors (Chang *et al.*, 2000; Shay and Roninson, 2004; Yun *et al.*, 2009), reinforcing the therapeutic relevance of prosenescence cancer therapy using SAC modulators. Together with their cell-autonomous activity, such potential backup interactions between senescence and cell death through mitotic catastrophe might provide additional justification for AURKB inhibitors or other SAC modulators as a therapeutic module in cancer.

MATERIALS AND METHODS

Cell culture and gene transfer

IMR90 and BJ human fibroblasts (American Type Culture Collection [ATCC], Manassas, VA) were cultured in phenol red–free DMEM with 10% fetal bovine serum (FBS) under 5% oxygen as described previously (Young *et al.*, 2009). HeLa and H1299 cells (ATCC) were cultured in phenol red–free DMEM with 10% FBS. Retroviral gene transfer was carried out as described (Narita *et al.*, 2006). RAS-induced senescence was triggered by the addition of 4-hydroxytamoxifen to cells expressing H-RAS^{G12V} fused to the estrogen receptor ligand-binding domain (ER:RAS; Young *et al.*, 2009). Quiescence was induced by incubating cells in DMEM with 0.1% serum for 3 d.

Plasmids

The following retroviral plasmids were used: pLNCX2 (*ER:HRAS^{G12V}* [*ER:RAS*]; Young *et al.*, 2009), pWZL-hygro (*EGFP*, *EGFP:AURKB*, *EDFP:AURKB^{D218N}*). miR30-based short hairpin RNA was expressed from pMSCV-puro (*sh-AURKB*, *sh-p53*; Silva *et al.*, 2005). The following target sequences were used for pMSCV-miR30-*AURKB*: gaagggatccctaactgtt (#1), tttgtttaataaaggctga (#2), ggtccctgtcattcactcg (#3), and actgttccctatctgtt (#4). Sh-p53 was previously described as sh-p53#2 (Kirschner *et al.*, 2015).

Antibodies

Antibodies used for Western blotting were as follows: cyclin A (C4710; Sigma-Aldrich, St. Louis, MO), cyclin B1 (4135; Cell Signaling, Beverly, MA), cyclin D1 (2926; Cell Signaling), p16 (sc-759; Santa Cruz Biotechnology, Dallas, TX), p21 (sc-397; Santa Cruz Biotechnology), p53 (sc-126; Santa Cruz Biotechnology), HMGA2 (sc-30223; Santa Cruz Biotechnology), H3S10phos (ab14955; Abcam, Cambridge, UK), histone H3 (ab1791; Abcam), AURKB (ab2254; Abcam), β-actin (A5441; Sigma-Aldrich), Rb (9309; Cell Signaling), LMNA/C (sc-7292; Santa Cruz Biotechnology), LMNB1 (ab16048; Abcam), IL-6 (MAB2061; R&D Systems, Minneapolis, MN), IL-8 (MAB208, R&D Systems), and MMP3 (a kind gift from Gillian Murphy, University of Cambridge, Cambridge, United Kingdom; Allan *et al.*, 1991).

Compound screening

IMR90 cells were plated in a 96-well plate (353948; BD Falcon, Franklin Lakes, NJ) at 10,000 cells/well. After 24 h, the medium was replaced by those containing 3 or 5 μM kinase inhibitors (InhibitorSelect kinase inhibitor library including 160 compounds; Calbiochem/Merck, Darmstadt, Germany). At 4 d after compound addition, cells were washed with phosphate-buffered saline (PBS), fixed in PBS with 4% paraformaldehyde for 15 min, and washed with PBS three times. Fixed cells were stained with 1 μg/ml DAPI in PBS (+0.2% Triton X-100) for 5 min. Images of the nuclei were captured and analyzed by ArrayScan (Thermo Scientific, Waltham, MA) with the settings shown in Supplemental Table S1. Briefly, nuclear contour was first determined (channel 1), and then spotty structures overlapping with the nuclei were identified (channel 2). Longer and shorter exposure times with the same filter set were applied for the channels 1 and 2, respectively. To rank the compounds by nuclear size and spottiness, the parameters Relative Nuclear Average Area and Relative Spot Total Area per Nucleus over DMSO control were used for the analyses, respectively. The compounds that gave a count of <100 nuclei/well were categorized as toxic and excluded from analyses. Hit compounds from each category were further narrowed and recategorized by visual inspection.

Compounds

The final concentrations used for the compound were as follows. For HDFs and H1299 cells, Aurora kinase inhibitor II, 8 μM (CAS# 331770-21-9; 189404; Merck); Cdk2 inhibitor IV, NU6140, 4 μM (CAS# 444723-13-1; 238804; Merck); PDGFR tyrosine kinase inhibitor V, 8 μM (CAS# 347155-76-4; 521234; Merck); Rho kinase inhibitor IV, 10 μM (555554, Merck; or CAS# 913844-45-8; 2485, Tocris, Bristol, UK); SU6656, 10 μM (CAS# 330161-87-0; 572635; Merck); ZM1 (ZM-447439), 2 μM (CAS# 331771-20-1; sc-200696, Santa Cruz Biotechnology); EGFR inhibitor, 0.5 μM (CAS# 879127-07-8; 324674; Merck); JNK inhibitor IX, 0.5 μM (CAS# 312917-14-9; 420136, Merck); MK2a inhibitor, 0.7 μM (CAS# 41179-33-3; 475863, Merck); and AZD1152-HQPA, 0.5 μM (CAS# 722544-51-6; SML0268, Sigma-Aldrich). For HeLa cells, Rho kinase inhibitor IV, Cdk2 inhibitor IV, and ZM1 were used at concentrations of 1.5, 4, and 1.5 μM, respectively. Nocodazole, 200 ng/ml (CAS# 31430-18-9; 487928; Merck); paclitaxel, 10 μM (CAS# 33069-62-4; T7402; Sigma-Aldrich).

Senescence and viability assays

Cells were treated with the hit compounds for 4 d (d4), followed by 5-d incubation in compound-free medium (d9) unless stated otherwise. BrdU incorporation, SA-β-gal, and colony formation assays were conducted as described (Narita *et al.*, 2003). The primary antibody for BrdU incorporation was 555627 (Becton Dickinson, Franklin Lakes, NJ). Cell viability was determined by trypan blue exclusion.

Immunofluorescence and laser scanning cytometer

Immunofluorescence was performed as described (Narita *et al.*, 2003). Primary antibodies were H3K9me3 (07-523; Millipore), H3K36me3 (13C9; Chandra *et al.*, 2012), LMNA (sc-20680; Santa Cruz Biotechnology), LMNA/C (sc-7292; Santa Cruz Biotechnology), LMNB1 (ab16048; Abcam), and α-tubulin (T5168, Sigma-Aldrich). Images were acquired with confocal (when stated) or wide-field fluorescence microscopy. LSC (iCys; Compucyte, Westwood, MA) was used to determine cell cycle profile and nuclear size distribution.

Live-cell imaging

IMR90 cells stably expressing histone H2B:EYFP were synchronized at the G1/S border using a double-thymidine treatment. Briefly, cells were plated at a density of 1.76×10^4 cells (in 300 μl of medium) per well onto an eight-well μ-slide (80826; ibidi, Martinsried, Germany). One day after plating, the medium was replaced with one containing 2 mM thymidine and incubated for 14 h. Cells were washed three times with 200 μl of prewarmed PBS and released into thymidine-free medium for 12 h. Then the cells were again incubated 13 h in the medium containing thymidine. These synchronized cells were washed three times with 200 μl of prewarmed PBS

and released into medium containing the compounds. Ten hours later, imaging was started and continued for ~5 h (5-min intervals) with an Eclipse TE2000 PFS Color microscope (Nikon, Tokyo, Japan). Conditions for the imaging were as follows: 10× objective; three focal planes, 3 µm apart; three fields per well; exposure time for bright field, 20 ms, and for YFP, 400 ms; gain, 13.6×; and ND filter, 1. Movie and individual files were processed by NIS-Elements software and ImageJ 1.48s (National Institutes of Health, Bethesda, MD).

In vitro kinase assay

The IC_{50} of the compounds was identified using a Z′-LYTE in vitro kinase assay and was carried out by the SelectScreen biochemical kinase profiling service (Invitrogen, Carlsbad, CA). The assay was conducted at 10 points from 1 nM to 2 mM with the ATP concentration 10 µM for AURKA and 81 µM for AURKB.

ACKNOWLEDGMENTS

We thank F. Gergely, V. M. Draviam, T. Toda, and P. Parker for thoughtful discussions, S. H. Lee for critical reading and discussions, and the Cambridge Institute Core Microscopy Facility (A. Schreiner, H. Zecchini, and L. Berry) and Cancer Research Technology Discovery Laboratories for technical support. This work was supported by the University of Cambridge, Cancer Research UK, Hutchison Whampoa; Cancer Research UK Grants A6691 and A9892 (M.N., N.K., C.J.T., D.C.B., C.J.C., L.S.G., and M.S.); and a fellowship from the Uehara Memorial Foundation (M.S.).

REFERENCES

Acosta JC, O'Loghlen A, Banito A, Guijarro MV, Augert A, Raguz S, Fumagalli M, Da Costa M, Brown C, Popov N, *et al.* (2008). Chemokine signaling via the CXCR2 receptor reinforces senescence. Cell 133, 1006–1018.

Acosta JC, Gil J (2012). Senescence: a new weapon for cancer therapy. Trends Cell Biol 22, 211–219.

Allan JA, Hembry RM, Angal S, Reynolds JJ, Murphy G (1991). Binding of latent and high Mr active forms of stromelysin to collagen is mediated by the C-terminal domain. J Cell Sci 99, 789–795.

Andreassen PR, Lohez OD, Lacroix FB (2001). Tetraploid state induces p53-dependent arrest of nontransformed mammalian cells in G1. Mol Biol Cell 12, 1315–1328.

Bain J, Plater L, Elliott M, Shpiro N, Hastie CJ, McLauchlan H, Klevernic I, Arthur JSC, Alessi DR, Cohen P (2007). The selectivity of protein kinase inhibitors: a further update. Biochem J 408, 297–315.

Barascu A, Le Chalony C, Pennarun G, Genet D, Imam N, Lopez B, Bertrand P (2012). Oxidative stress induces an ATM-independent senescence pathway through p38 MAPK-mediated lamin B1 accumulation. EMBO J 31, 1080–1094.

Bemiller PM, Lee LH (1978). Nucleolar changes in senescing WI-38 cells. Mech Ageing Dev 8, 417–427.

Bischof O, Kirsh O, Pearson M, Itahana K, Pelicci PG, Dejean A (2002). Deconstructing PML-induced premature senescence. EMBO J 21, 3358–3369.

Bischof O, Nacerddine K, Dejean A (2005). Human papillomavirus oncoprotein E7 targets the promyelocytic leukemia protein and circumvents cellular senescence via the Rb and p53 tumor suppressor pathways. Mol Cell Biol 25, 1013–1024.

Cairney CJ, Bilsland AE, Evans TRJ, Roffey J, Bennett DC, Narita M, Torrance CJ, Keith WN (2012). Cancer cell senescence: a new frontier in drug development. Drug Discov Today 17, 269–276.

Campisi J (2013). Aging, cellular senescence, and cancer. Annu Rev Physiol 75, 685–705.

Carmena M, Wheelock M, Funabiki H, Earnshaw WC (2012). The chromosomal passenger complex (CPC): from easy rider to the godfather of mitosis. Nat Rev Mol Cell Biol 13, 789–803.

Chandra T, Kirschner K, Thuret J-Y, Pope BD, Ryba T, Newmann S, Ahmed K, Samarajiwa SA, Salama R, Carroll T, *et al.* (2012). Independence of repressive histone marks and chromatin compaction during senescent heterochromatic layer formation. Mol Cell 47, 203–214.

Chang BD, Broude EV, Fang J, Kalinichenko TV, Abdryashitov R, Poole JC, Roninson IB (2000). p21Waf1/Cip1/Sdi1-induced growth arrest is associated with depletion of mitosis-control proteins and leads to abnormal mitosis and endoreduplication in recovering cells. Oncogene 19, 2165–2170.

Chang BD, Swift ME, Shen M, Fang J, Broude EV, Roninson IB (2002). Molecular determinants of terminal growth arrest induced in tumor cells by a chemotherapeutic agent. Proc Natl Acad Sci USA 99, 389–394.

Chuprin A, Gal H, Biron-Shental T, Biran A, Amiel A, Rozenblatt S, Krizhanovsky V (2013). Cell fusion induced by ERVWE1 or measles virus causes cellular senescence. Genes Dev 27, 2356–2366.

Coppé JP, Desprez PY, Krtolica A, Campisi J (2010). The senescence-associated secretory phenotype: the dark side of tumor suppression. Annu Rev Pathol 5, 99–118.

Correia-Melo C, Hewitt G, Passos JF (2014). Telomeres, oxidative stress and inflammatory factors: partners in cellular senescence? Longev Healthspan 3, 1.

Cristofalo VJ, Pignolo RJ (1993). Replicative senescence of human fibroblast-like cells in culture. Physiol Rev 73, 617–638.

Davoli T, de Lange T (2011). The causes and consequences of polyploidy in normal development and cancer. Annu Rev Cell Dev Biol 27, 585–610.

Davoli T, Denchi EL, de Lange T (2010). Persistent telomere damage induces bypass of mitosis and tetraploidy. Cell 141, 81–93.

Dimri GP, Lee X, Basile G, Acosta M, Scott G, Roskelley C, Medrano EE, Linskens M, Rubelj I, Pereira-Smith O (1995). A biomarker that identifies senescent human cells in culture and in aging skin in vivo. Proc Natl Acad Sci USA 92, 9363–9367.

Ditchfield C, Johnson VL, Tighe A, Ellston R, Haworth C, Johnson T, Mortlock A, Keen N, Taylor SS (2003). Aurora B couples chromosome alignment with anaphase by targeting BubR1, Mad2, and Cenp-E to kinetochores. J Cell Biol 161, 267–280.

Dreesen O, Chojnowski A, Ong PF, Zhao TY, Common JE, Lunny D, Lane EB, Lee SJ, Vardy LA, Stewart CL, *et al.* (2013). Lamin B1 fluctuations have differential effects on cellular proliferation and senescence. J Cell Biol 200, 605–617.

Dörr JR, Yu Y, Milanovic M, Beuster G, Zasada C, Dabritz HM, Lisec J, Lenze D, Gerhardt A, Schleicher K, *et al.* (2013). Synthetic lethal metabolic targeting of cellular senescence in cancer therapy. Nature 501, 421–425.

Ermis A, Oberringer M, Wirbe R, Koschnick M, Mutschler W, Hanselmann RG (1998). Tetraploidization is a physiological enhancer of wound healing. Eur Surg Res 30, 385–392.

Ewald JA, Desotelle JA, Wilding G, Jarrard DF (2010). Therapy-induced senescence in cancer. J Natl Cancer Inst 102, 1536–1546.

Ewald JA, Peters N, Desotelle JA, Hoffmann FM, Jarrard DF (2009). A high-throughput method to identify novel senescence-inducing compounds. J Biomol Screen 14, 853–858.

Ferbeyre G, de Stanchina E, Querido E, Baptiste N, Prives C, Lowe SW (2000). PML is induced by oncogenic ras and promotes premature senescence. Genes Dev 14, 2015–2027.

Freund A, Laberge RM, Demaria M, Campisi J (2012). Lamin B1 loss is a senescence-associated biomarker. Mol Biol Cell 23, 2066–2075.

Fujiwara T, Bandi M, Nitta M, Ivanova EV, Bronson RT, Pellman D (2005). Cytokinesis failure generating tetraploids promotes tumorigenesis in p53-null cells. Nature 437, 1043–1047.

Funayama R, Saito M, Tanobe H, Ishikawa F (2006). Loss of linker histone H1 in cellular senescence. J Cell Biol 175, 869–880.

Ganem NJ, Cornils H, Chiu SY, O'Rourke KP, Arnaud J, Yimlamai D, Théry M, Camargo FD, Pellman D (2014). Cytokinesis failure triggers hippo tumor suppressor pathway activation. Cell 158, 833–848.

Ganem NJ, Storchova Z, Pellman D (2007). Tetraploidy, aneuploidy and cancer. Curr Opin Genet Dev 17, 157–162.

Gascoigne KE, Taylor SS (2009). How do anti-mitotic drugs kill cancer cells? J Cell Sci 122, 2579–2585.

Gautschi O, Heighway J, Mack PC, Purnell PR, Lara PN, Gandara DR (2008). Aurora kinases as anticancer drug targets. Clin Cancer Res 14, 1639–1648.

Gentric G, Desdouets C, Celton-Morizur S (2012). Hepatocytes polyploidization and cell cycle control in liver physiopathology. Int J Hepatol 2012, 282430–282438.

Gewirtz DA., Holt SE, Elmore LW (2008). Accelerated senescence: an emerging role in tumor cell response to chemotherapy and radiation. Biochem Pharmacol 76, 947–957.

Gil J, Bernard D, Martínez D, Beach D (2004). Polycomb CBX7 has a unifying role in cellular lifespan. Nat Cell Biol 6, 67–72.

Girdler F, Gascoigne KE, Eyers PA, Hartmuth S, Taylor SS (2006). Validating Aurora B as an anti-cancer drug target. J Cell Sci 119, 3664–3675.
Gizatullin F, Yao Y, Kung V, Harding MW, Loda M, Shapiro GI (2006). The Aurora kinase inhibitor VX-680 induces endoreduplication and apoptosis preferentially in cells with compromised p53-dependent postmitotic checkpoint function. Cancer Res 66, 7668–7677.
Goldenson B, Crispino JD (2015). The aurora kinases in cell cycle and leukemia. Oncogene 34, 537–545.
Goldstein S (1990). Replicative senescence: the human fibroblast comes of age. Science 249, 1129–1133.
Green MR, Woolery JE, Mahadevan D (2011). Update on Aurora kinase targeted therapeutics in oncology. Expert Opin Drug Discov 6, 291–307.
Gully CP, Velazquez-Torres G, Shin J-H, Fuentes-Mattei E, Wang E, Carlock C, Chen J, Rothenberg D, Adams HP, Choi HH, *et al.* (2012). Aurora B kinase phosphorylates and instigates degradation of p53. Proc Natl Acad Sci USA 109, E1513–E1522.
Hardwicke MA, Oleykowski CA, Plant R, Wang J, Liao Q, Moss K, Newlander K, Adams JL, Dhanak D, Yang J, *et al.* (2009). GSK1070916, a potent Aurora B/C kinase inhibitor with broad antitumor activity in tissue culture cells and human tumor xenograft models. Mol Cancer Ther 8, 1808–1817.
Hauf S, Cole RW, LaTerra S, Zimmer C, Schnapp G, Walter R, Heckel A, van Meel J, Rieder CL, Peters JM (2003). The small molecule Hesperadin reveals a role for Aurora B in correcting kinetochore-microtubule attachment and in maintaining the spindle assembly checkpoint. J Cell Biol 161, 281–294.
Hayashi MT, Karlseder J (2013). DNA damage associated with mitosis and cytokinesis failure. Oncogene 32, 4593–4601.
Huck JJ, Zhang M, McDonald A, Bowman D, Hoar KM, Stringer B, Ecsedy J, Manfredi MG, Hyer ML (2010). MLN8054, an inhibitor of Aurora A kinase, induces senescence in human tumor cells both in vitro and in vivo. Mol Cancer Res 8, 373–384.
Jackson JG, Pant V, Li Q, Chang LL, Quintas-Cardama A, Garza D, Tavana O, Yang P, Manshouri T, Li Y, *et al.* (2012). p53-mediated senescence impairs the apoptotic response to chemotherapy and clinical outcome in breast cancer. Cancer Cell 21, 793–806.
Jacobs JJ, Keblusek P, Robanus-Maandag E, Kristel P, Lingbeek M, Nederlof PM, van Welsem T, van de Vijver MJ, Koh EY, Daley GQ, *et al.* (2000). Senescence bypass screen identifies TBX2, which represses Cdkn2a (p19(ARF)) and is amplified in a subset of human breast cancers. Nat Genet 26, 291–299.
Johmura Y, Shimada M, Misaki T, Naiki-Ito A, Miyoshi H, Motoyama N, Ohtani N, Hara E, Nakamura M, Morita A, *et al.* (2014). Necessary and sufficient role for a mitosis skip in senescence induction. Mol Cell 55, 73–84.
Jun JI, Lau LF (2010). The matricellular protein CCN1 induces fibroblast senescence and restricts fibrosis in cutaneous wound healing. Nat Cell Biol 12, 676–685.
Jung JE, Kim T-K, Lee J-S, Oh S-Y, Kwak S, Jin X, Sohn J-Y, Song M-K, Sohn Y-W, Lee S-Y, *et al.* (2005). Survivin inhibits anti-growth effect of p53 activated by aurora B. Biochem Biophys Res Commun 336, 1164–1171.
Kaestner P, Stolz A, Bastians H (2009). Determinants for the efficiency of anticancer drugs targeting either Aurora-A or Aurora-B kinases in human colon carcinoma cells. Mol Cancer Ther 8, 2046–2056.
Kang TW, Yevsa T, Woller N, Hoenicke L, Wuestefeld T, Dauch D, Hohmeyer A, Gereke M, Rudalska R, Potapova A, *et al.* (2011). Senescence surveillance of pre-malignant hepatocytes limits liver cancer development. Nature 479, 547–551.
Keen N, Taylor S (2004). Aurora-kinase inhibitors as anticancer agents. Nat Rev Cancer 4, 927–936.
Keen N, Taylor S (2009). Mitotic drivers—inhibitors of the Aurora B kinase. Cancer Metastasis Rev 28, 185–195.
Kelly AE, Funabiki H (2009). Correcting aberrant kinetochore microtubule attachments: an Aurora B-centric view. Curr Opin Cell Biol 21, 51–58.
Kim HJ, Cho JH, Quan H, Kim JR (2011). Down-regulation of Aurora B kinase induces cellular senescence in human fibroblasts and endothelial cells through a p53-dependent pathway. FEBS Lett 585, 3569–3576.
Kirschner K, Samarajiwa SA, Cairns JM, Menon S, Perez-Mancera PA, Tomimatsu K, Bermejo-Rodriguez C, Ito Y, Chandra T, Narita M, *et al.* (2015). Phenotype specific analyses reveal distinct regulatory mechanism for chronically activated p53. PLoS Genet 11, e1005053.
Kortlever RM, Brummelkamp TR, van Meeteren LA, Moolenaar WH, Bernards R (2008). Suppression of the p53-dependent replicative senescence response by lysophosphatidic acid signaling. Mol Cancer Res 6, 1452–1460.
Krenning L, Feringa FM, Shaltiel IA, van den Berg J, Medema RH (2014). Transient activation of p53 in G2 phase is sufficient to induce senescence. Mol Cell 55, 59–72.
Krizhanovsky V, Yon M, Dickins RA, Hearn S, Simon J, Miething C, Yee H, Zender L, Lowe SW (2008). Senescence of activated stellate cells limits liver fibrosis. Cell 134, 657–667.
Kuilman T, Peeper DS (2009). Senescence-messaging secretome: SMS-ing cellular stress. Nat Rev Cancer 9, 81–94.
Lahtela J, Corson LB, Hemmes A, Brauer MJ, Koopal S, Lee J, Hunsaker TL, Jackson PK, Verschuren EW (2013). A high-content cellular senescence screen identifies candidate tumor suppressors, including EPHA3. Cell Cycle 12, 625–634.
Leal JFM, Fominaya J, Cascon A, Guijarro MV, Blanco-Aparicio C, Lleonart M, Castro ME, Cajal SRY, Robledo M, Beach DH, *et al.* (2008). Cellular senescence bypass screen identifies new putative tumor suppressor genes. Oncogene 27, 1961–1970.
Lens SMA, Voest EE, Medema RH (2010). Shared and separate functions of polo-like kinases and aurora kinases in cancer. Nat Rev Cancer 10, 825–841.
Li W, Anderson RA (2014). Star-PAP controls HPV E6 regulation of p53 and sensitizes cells to VP-16. Oncogene 33, 928–932.
Liu Y, Hawkins OE, Su Y, Vilgelm AE, Sobolik T, Thu Y-M, Kantrow S, Splittgerber RC, Short S, Amiri KI, *et al.* (2013). Targeting aurora kinases limits tumour growth through DNA damage-mediated senescence and blockade of NF-κB impairs this drug-induced senescence. EMBO Mol Med 5, 149–166.
López-Otín C, Blasco MA, Partridge L, Serrano M, Kroemer G (2013). The hallmarks of aging. Cell 153, 1194–1217.
Macleod KF, Sherry N, Hannon G, Beach D, Tokino T, Kinzler K, Vogelstein B, Jacks T (1995). p53-dependent and independent expression of p21 during cell growth, differentiation, and DNA damage. Genes Dev 9, 935–944.
Maeshima K, Yahata K, Sasaki Y, Nakatomi R, Tachibana T, Hashikawa T, Imamoto F, Imamoto N (2006). Cell-cycle-dependent dynamics of nuclear pores: pore-free islands and lamins. J Cell Sci 119, 4442–4451.
Margolis RL, Lohez OD, Andreassen PR (2003). G1 tetraploidy checkpoint and the suppression of tumorigenesis. J Cell Biochem 88, 673–683.
Matsumura T, Zerrudo Z, Hayflick L (1979). Senescent human diploid cells in culture: survival, DNA synthesis and morphology. J Gerontol 34, 328–334.
Mitsui Y, Schneider EL (1976). Increased nuclear sizes in senescent human diploid fibroblast cultures. Exp Cell Res 100, 147–152.
Muñoz-Espín D, Canamero M, Maraver A, Gómez-López G, Contreras J, Murillo-Cuesta S, Rodriguez-Baeza A, Varela-Nieto I, Ruberte J, Collado M, Serrano M (2013). Programmed cell senescence during mammalian embryonic development. Cell 155, 1104–1118.
Narita M, Narita M, Krizhanovsky V, Nuñez S, Chicas A, Hearn SA, Myers MP, Lowe SW (2006). A novel role for high-mobility group a proteins in cellular senescence and heterochromatin formation. Cell 126, 503–514.
Narita M, Nuñez S, Heard E, Narita M, Lin AW, Hearn SA, Spector DL, Hannon GJ, Lowe SW (2003). Rb-mediated heterochromatin formation and silencing of E2F target genes during cellular senescence. Cell 113, 703–716.
Panopoulos A, Pacios-Bras C, Choi J, Yenjerla M, Sussman MA, Fotedar R, Margolis RL (2014). Failure of cell cleavage induces senescence in tetraploid primary cells. Mol Biol Cell 25, 3105–3118.
Pearson M, Carbone R, Sebastiani C, Cioce M, Fagioli M, Saito S, Higashimoto Y, Appella E, Minucci S, Pandolfi PP, *et al.* (2000). PML regulates p53 acetylation and premature senescence induced by oncogenic Ras. Nature 406, 207–210.
Pérez-Mancera PA, Young ARJ, Narita M (2014). Inside and out: the activities of senescence in cancer. Nat Rev Cancer 14, 547–558.
Poele te RH, Okorokov AL, Jardine L, Cummings J, Joel SP (2002). DNA damage is able to induce senescence in tumor cells in vitro and in vivo. Cancer Res 62, 1876–1883.
Rovillain E, Mansfield L, Lord CJ, Ashworth A, Jat PS (2011). An RNA interference screen for identifying downstream effectors of the p53 and pRB tumour suppressor pathways involved in senescence. BMC Genomics 12, 355.
Sadaie M, Salama R, Carroll T, Tomimatsu K, Chandra T, Young ARJ, Narita M, Perez-Mancera PA, Bennett DC, Chong H, *et al.* (2013). Redistribution of the Lamin B1 genomic binding profile affects rearrangement

of heterochromatic domains and SAHF formation during senescence. Genes Dev 27, 1800–1808.
Salama R, Sadaie M, Hoare M, Narita M (2014). Cellular senescence and its effector programs. Genes Dev 28, 99–114.
Schmitt CA, Fridman JS, Yang M, Lee S, Baranov E, Hoffman RM, Lowe SW (2002). A senescence program controlled by p53 and p16INK4a contributes to the outcome of cancer therapy. Cell 109, 335–346.
Serrano M, Lin AW, McCurrach ME, Beach D, Lowe SW (1997). Oncogenic ras provokes premature cell senescence associated with accumulation of p53 and p16INK4a. Cell 88, 593–602.
Shah PP, Donahue G, Otte GL, Capell BC, Nelson DM, Cao K, Aggarwala V, Cruickshanks HA, Rai TS, McBryan T, *et al.* (2013). Lamin B1 depletion in senescent cells triggers large-scale changes in gene expression and the chromatin landscape. Genes Dev 27, 1787–1799.
Shay JW, Roninson IB (2004). Hallmarks of senescence in carcinogenesis and cancer therapy. Oncogene 23, 2919–2933.
Shay JW, Wright WE (2005). Senescence and immortalization: role of telomeres and telomerase. Carcinogenesis 26, 867–874.
Shimi T, Butin-Israeli V, Adam SA, Hamanaka RB, Goldman AE, Lucas CA, Shumaker DK, Kosak ST, Chandel NS, Goldman RD (2011). The role of nuclear lamin B1 in cell proliferation and senescence. Genes Dev 25, 2579–2593.
Shvarts A, Brummelkamp TR, Scheeren F, Koh E, Daley GQ, Spits H, Bernards R (2002). A senescence rescue screen identifies BCL6 as an inhibitor of anti-proliferative p19(ARF)-p53 signaling. Genes Dev 16, 681–686.
Silva JM, Li MZ, Chang K, Ge W, Golding MC, Rickles RJ, Siolas D, Hu G, Paddison PJ, Schlabach MR, *et al.* (2005). Second-generation shRNA libraries covering the mouse and human genomes. Nat Genet 37, 1281–1288.
Storchova Z, Kuffer C (2008). The consequences of tetraploidy and aneuploidy. J Cell Sci 121, 3859–3866.
Storer M, Mas A, Robert-Moreno A, Pecoraro M, Ortells C, Giacomo VD, Yosef R, Pilpel N, Krizhanovsky V, Sharpe J, *et al.* (2013). Senescence is a developmental mechanism that contributes to embryonic growth and patterning. Cell 155, 1119–1130.
Uetake Y, Sluder G (2004). Cell cycle progression after cleavage failure: mammalian somatic cells do not possess a "tetraploidy checkpoint." J Cell Biol 165, 609–615.
Vitale I, Galluzzi L, Castedo M, Kroemer G (2011). Mitotic catastrophe: a mechanism for avoiding genomic instability. Nat Rev Mol Cell Biol 12, 385–392.
Wesierska-Gadek J, Schloffer D, Kotala V, Horky M (2002). Escape of p53 protein from E6-mediated degradation in HeLa cells after cisplatin therapy. Int J Cancer 101, 128–136.
Wilkinson RW, Odedra R, Heaton SP, Wedge SR, Keen NJ, Crafter C, Foster JR, Brady MC, Bigley A, Brown E, *et al.* (2007). AZD1152, a selective inhibitor of Aurora B kinase, inhibits human tumor xenograft growth by inducing apoptosis. Clin Cancer Res 13, 3682–3688.
Wong C, Stearns T (2005). Mammalian cells lack checkpoints for tetraploidy, aberrant centrosome number, and cytokinesis failure. BMC Cell Biol 6, 6.
Xue W, Zender L, Miething C, Dickins RA, Hernando E, Krizhanovsky V, Cordón-Cardo C, Lowe SW (2007). Senescence and tumour clearance is triggered by p53 restoration in murine liver carcinomas. Nature 445, 656–660.
Yang J, Ikezoe T, Nishioka C, Tasaka T, Taniguchi A, Kuwayama Y, Komatsu N, Bandobashi K, Togitani K, Koeffler HP, *et al.* (2007). AZD1152, a novel and selective aurora B kinase inhibitor, induces growth arrest, apoptosis, and sensitization for tubulin depolymerizing agent or topoisomerase II inhibitor in human acute leukemia cells in vitro and in vivo. Blood 110, 2034–2040.
Young ARJ, Narita M, Ferreira M, Kirschner K, Sadaie M, Darot JFJ, Tavare S, Arakawa S, Shimizu S, Watt FM, *et al.* (2009). Autophagy mediates the mitotic senescence transition. Genes Dev 23, 798–803.
Yun M, Han Y-H, Yoon SH, Kim HY, Kim B-Y, Ju Y-J, Kang C-M, Jang SH, Chung H-Y, Lee S-J, *et al.* (2009). p31comet Induces cellular senescence through p21 accumulation and Mad2 disruption. Mol Cancer Res 7, 371–382.
Zhang R, Poustovoitov MV, Ye X, Santos HA, Chen W, Daganzo SM, Erzberger JP, Serebriiskii IG, Canutescu AA, Dunbrack RL, *et al.* (2005). Formation of MacroH2A-containing senescence-associated heterochromatin foci and senescence driven by ASF1a and HIRA. Dev Cell 8, 19–30.